Analysis of a strong mass-based flame stretch model for turbulent premixed combustion

Analysis of a strong mass-based flame stretch model for turbulent premixed combustion

R. J. M. Bastiaans,[a] J. A. van Oijen, and L. P. H. de Goey
Department of Mechanical Engineering, Combustion Technology Section, Eindhoven University of Technology, P.O. Box 513, 5600 MB Eindhoven, The Netherlands

(Received 3 September 2008; accepted 4 November 2008; published online 15 January 2009)

In the present paper a theory describing effects of strong flame stretch on turbulent flame propagation [L. P. H. de Goey and J. H. M. ten Thije Boonkkamp, "A flamelet description of premixed laminar flames and the relation with flame stretch," Combust. Flame **119**, 253 (1999)] is extended to volume averaged quantities and validated with direct numerical simulation (DNS). The extended theory describes the fuel consumption rate in terms of subgrid scale contributions connected to propagation effects including strong flame stretch. In case there is no preferential diffusion present, it is predicted that the total consumption rate is not affected by local stretch at all. Then the total consumption is described by the unstretched mass burning rate multiplied with the flame surface density. DNSs of turbulent flame kernels have been carried out in order to support the results from the theory. The chemistry is described by application of the flamelet generated manifold technique. The strong stretch theory is shown to be valid up to realizations in the thin reaction zone regime by three independent methods. The local effects of stretch are described, evaluated, and interpreted. Locally the mass burning rate changes by fuel leakage tangential to the flame, but this has no integral effect. The method can be used for subgrid scale modeling of turbulent flame propagation. © *2009 American Institute of Physics*. [DOI: 10.1063/1.3059616]

I. INTRODUCTION

Flame stretch is an important parameter that is recognized to have an important effect on the consumption rate of premixed flames. By using asymptotic theory, first relations between burning velocity and flame stretch were already given in Refs. 1 and 2. However, these theories are only valid for weak stretch, i.e., for Karlovitz numbers much smaller than unity. This study focuses on the strong stretch theory of De Goey and ten Thije Boonkkamp[3] for Karlovitz number on the order of 1 or slightly larger. This theory was proven to be very accurate also for high stretch rates. Therefore, it could initiate a more accurate implementation of the effects of stretch in turbulent flame models. The laminar burning velocity, which is largely affected by stretch, is an important parameter for modeling turbulent combustion. Flame stretch is also responsible for the creation of flame surface area, affecting the consumption rate as well. In the case of turbulent reacting flows, stretch rates vary significantly in space and time. In turbulence modeling the local flame stretch is unknown and the effect of flame stretch has to be modeled.

In this paper the strong stretch model of Ref. 3 is extended to volume averaged quantities as used in large eddy simulations (LESs). Furthermore, this extension is validated by means of an analysis of direct numerical simulations (DNSs). The simulations are direct in the sense that the smallest scales of motion are fully resolved, while the chemical kinetics are solved in advance and parametrized in a table by using the flamelet generated manifold technique (FGM),[4] also known as flame prolongation of intrinsic low dimensional manifolds (ILDM).[5] The state of the mixture is assumed to be directly linked to a few progress variables. The conservation equations for these progress variables are solved using DNS, with the unclosed terms coming from the table. This allows the use of detailed chemical kinetics without having to solve all the individual species conservation equations.

In the present study, only a single progress variable is used. In previous research,[6] it was shown that simulations of premixed methane air flames in the corrugated flamelet regime by means of a single progress variable results in accurate predictions of the local mass burning rate. In additional research,[7] flamelets were sampled from turbulent realizations of DNS-FGM simulations on the basis of a single progress variable. These flamelets were analyzed by back-substitution in a one-dimensional (1D) detailed chemistry code including the local stretch and curvature. The analysis supported the previous conclusion. Furthermore, in a more recent research paper,[8] two-dimensional (2D) manifolds were used and evaluated. In this paper it was found that the accuracy of the mass burning rate can even be improved by an order of magnitude by adding an additional progress variable.

The approach that is followed here requires the validity of a flamelet regime, i.e., that flame structures are quasi-1D structures, because the smallest hydrodynamic structures are not able to penetrate the reaction zone of the flame. This is indicated by the Karlovitz number (e.g., Ref. 9),

[a]Author to whom correspondence should be addressed. Fax: +31 40 2433445. Electronic mail: r.j.m.bastiaans@tue.nl.

$$\mathrm{Ka} = \frac{\delta_f^2}{\eta^2}, \tag{1}$$

with δ_f being the flame thickness, as defined by the maximal gradient of temperature, and η the Kolmogorov scale of the flow. For Karlovitz numbers in the lower regions of the thin reaction zone regime, as defined by, e.g., Peters,[9] it is proven that this is still true (see, e.g.,[10,11]). Experimental evidence is also provided by de Goey *et al.*[12] and on a numerical basis it was also reported in Refs. 6, 7, and 13. So for the flamelet assumption and the present analysis to be true the Karlovitz number can be 1 or larger. Then combustion takes place under strong stretch conditions. For technical applications this is a very important mode of premixed turbulent combustion. Following Ref. 3, in this study we will frequently use the (local) Karlovitz integral, $\mathcal{K}a$, defined in the next section, and its statistical mean value $\langle \mathcal{K}a \rangle$, i.e., the Karlovitz integral averaged over the turbulent flame surface. As the Karlovitz integral approaches unity, somewhere in the thin reaction zone regime, the flamelet assumption gets violated. This corresponds to Karlovitz numbers Ka larger than 1.

There have been many investigations on flame stretch and dynamics of flame kernels subjected to different perturbations; for some recent investigations see Refs. 14–22. However, the goal of the present study is to demonstrate that the total consumption rate is determined by the product of the unstretched mass burning rate and the flame surface density for Lewis numbers equal to unity. This was already observed, e.g., in a 2D context with single step chemistry by Haworth and Poinsot.[23] In the paper of Bilger *et al.*,[24] discussing Damköhler's paradigm of turbulent premixed combustion, they refer to the hypothesis of a turbulent propagation speed being equal to the laminar (unstretched) burning velocity multiplied by the actual flame surface divided by the projected surface. The present result shows that this is not only a hypothesis (for Le=1). Moreover, to our knowledge the present result was never derived rigorously. As stated in Ref. 23 we will show indeed that "curvature effects cancel out when the mean flamelet speed (averaged along the flame front) is computed. Only flame strain effects persist to result in a mean flamelet speed that is identical to the laminar value for Le=1." In the present paper this result will be derived analytically. Moreover, the result will be supported by post-processing of 3D fully compressible DNS results.

So here we will look at the derivation and the different contributions that are involved. Based on this derivation a physical interpretation of the contributing effects will be given. Thus we will identify the ingredients of the strong stretch theory mentioned in terms of subgrid scale contributions for the consumption rate. This is supplemented with an evaluation of these terms based on DNS results. These results can facilitate the introduction of improved models for the effects of unresolved strong flame stretch. In the next section the flame stretch model is described in brief and details are given in Appendix A. Next the considered DNS cases to validate the model are described and results about the development of the flames are given and discussed. Thereafter, in an *a priori* evaluation, the new model is applied to the data and validated with directly calculated stretch effects. The paper ends with conclusions.

II. THE STRONG FLAME STRETCH MODEL

A. General description

We consider premixed combustion situated in the flamelet regime of turbulent combustion.[9] A flamelet is a relatively thin layer consisting of a preheat zone to which heat is added by means of diffusion from an even thinner reaction layer acting as the source of thermal energy. This means that the combustion process takes place in very thin, more or less 1D structures. The progress of the combustion process, ranging from an unburnt to a fully burnt state, is reflected by a progress variable $\mathcal{Y}$. Generally $\mathcal{Y}$ is normalized to the interval [0–1] and it can be defined by a suitable combination of chemical species, covering the entire flamelet including the preheat zone. A simple example would be the normalized concentration of carbon dioxide in the case of lean methane combustion. The assumption associated with the flamelet regime of turbulent combustion is that flame structures are locally still 1D although relatively small variations can occur. As an example, the area between isocontours of $\mathcal{Y}$ might have some variations due to stretch effects. Therefore, each value of $\mathcal{Y}$ has its own flame velocity u_i^f, as reflected in the kinematic equation that defines the u_i^f field,

$$\frac{\partial \mathcal{Y}}{\partial t} + u_i^f \frac{\partial \mathcal{Y}}{\partial x_i} \equiv 0. \tag{2}$$

To take the effects of flame stretch into account we follow Ref. 3. In this paper an expression for the stretch rate K is derived on a mass-based rather than on a (classical) surface-based definition. The equation for the local stretch rate reads

$$K = \frac{1}{M}\frac{dM}{dt}, \tag{3}$$

where M is the amount of mass in an arbitrary small control volume $V(t)$ moving with the flame velocity u_i^f,

$$M(t) = \int_{V(t)} \rho dV. \tag{4}$$

In the present definition of stretch, both strain and curvature are included. By application of the transport theorem to $M(t)$ in Eq. (4) the stretch field is obtained as

$$\rho K = \frac{\partial \rho}{\partial t} + \frac{\partial \rho u_i^f}{\partial x_i}, \tag{5}$$

which (with $S_d n_i = u_i^f - u_i$) finally gives

$$\rho K = \frac{\partial}{\partial x_i}(\rho S_d n_i). \tag{6}$$

Here n_i is the local normal vector to the flamelet progress isocontours $\mathcal{Y}$ and S_d is the local displacement speed of the specific $\mathcal{Y}$ isoplane. On the basis of this definition, a model for the influence of stretch and curvature on the mass burning rate, $m=\rho S_d$, has been developed, which also holds for

strong stretch in turbulent flames. In a numerical study,[25] it was shown that this model shows good agreement with calculations for spherically expanding laminar flames. This model, for the ratio of the actual mass burning rate at the inner layer, m_{in}, relative to the unperturbed mass burning rate at the inner layer, m_{in}^0, reads

$$\frac{m_{\mathrm{in}}}{m_{\mathrm{in}}^0} = 1 - \mathcal{K}a, \tag{7}$$

with the Karlovitz integral as determined by the distribution of flame stretch K of Eq. (3), surface area σ, and a progress variable $\mathcal{Y}$,

$$\mathcal{K}a := \frac{1}{\sigma_{\mathrm{in}} m_{\mathrm{in}}^0} \int_{s_u}^{s_b} \sigma \rho K \mathcal{Y} ds. \tag{8}$$

Equation (7) is a $\mathrm{Le}_i = 1$ contraction of the general case for $\mathrm{Le}_i \neq 1$ as described in Ref. 3 and is shown to be valid also for preferential diffusion effects in combination with weak stretch.[26] Due to the definition of the Karlovitz integral $\mathcal{K}a$, the mass burning rate, Eq. (7), has no higher order terms and therefore it is an exact result.

The Karlovitz integral, Eq. (8), describes local leakage of mass tangentially to the flame surface due to flow straining and curvature effects. The integral has to be taken over flamelet paths normal to the flame and s_u and s_b are the positions at the unburned side and the burned side, respectively. The local surface area σ is related to the local curvature κ, which is related to the normals n_i of the local $\mathcal{Y}$ isoplane,

$$\kappa = \frac{\partial n_i}{\partial x_i} = -\frac{1}{\sigma}\frac{\partial \sigma}{\partial s}, \tag{9}$$

with the normals

$$n_i = -\frac{\partial \mathcal{Y}/\partial x_i}{|\partial \mathcal{Y}/\partial x|}. \tag{10}$$

In turbulent premixed combustion the total fuel consumption rate is a result of the combined effect of flame surface increase and the local modulation of the mass burning rate. These effects will be studied in this paper.

The flame surface increase is reflected in the kinematic equation for the progress variable, Eq. (2), which can be written as

$$\frac{\partial \rho \mathcal{Y}}{\partial t} + \frac{\partial}{\partial x_i}(\rho u_i \mathcal{Y}) = -mn_i \frac{\partial \mathcal{Y}}{\partial x_i} = m\left|\frac{\partial \mathcal{Y}}{\partial x}\right| \equiv \Lambda. \tag{11}$$

This kinematic equation can be combined with a conservation equation for $\mathcal{Y}$ to yield an expression for the local mass burning rate,

$$m = \left(\frac{\partial}{\partial x_i}\left(\frac{\lambda}{\mathrm{Le}_{\mathcal{Y}}\, \bar{c}_p}\frac{\partial \mathcal{Y}}{\partial x_i}\right) + \dot{\omega}_{\mathcal{Y}}\right) \Bigg/ \left|\frac{\partial \mathcal{Y}}{\partial x}\right|, \tag{12}$$

and thus the stretch rate K can be determined from Eq. (6).

Flame propagation, Λ in Eq. (11), can be decomposed into a BML (Bray, Moss, and Libby) contribution connected to infinitely thin flames without stretch (as in Ref. 27) and a contribution associated with flame stretch inside the flame structure (the associated name giving will be clarified in Appendix A where we will discuss the turbulent case). These parts can be associated with a part in which the flame surface area is used and a part in which the local deviations of the mass burning rate due to flame stretch are present. The decomposition was made by applying Reynolds transport theorem to a fixed subvolume containing a propagating front. It can be written as

$$\Lambda = \Lambda^{\mathrm{BML}} + \Lambda^*, \tag{13}$$

in which

$$\Lambda^{\mathrm{BML}} = -\frac{\partial}{\partial x_i}(mn_i \mathcal{Y}) = -\rho K \mathcal{Y} + m\left|\frac{\partial \mathcal{Y}}{\partial x}\right| \tag{14}$$

and

$$\Lambda^* = \mathcal{Y}\frac{\partial}{\partial x_i}(mn_i) = \rho K \mathcal{Y}. \tag{15}$$

B. Application of an averaging procedure

In the case of LES, we apply a spatial filtering and Favre averaging,

$$\tilde{f} = \frac{\overline{\rho f}}{\bar{\rho}}, \tag{16}$$

to obtain

$$\frac{\partial \bar{\rho}\tilde{\mathcal{Y}}}{\partial t} + \frac{\partial}{\partial x_i}\widetilde{\bar{\rho} u_i \mathcal{Y}} = \bar{\Lambda}. \tag{17}$$

Then the turbulent decomposition results in primary variables on the left-hand side and the source term and unresolved turbulent fluxes on the right-hand side,

$$\frac{\partial \bar{\rho}\tilde{\mathcal{Y}}}{\partial t} + \frac{\partial}{\partial x_i}\bar{\rho}\tilde{u}_i\tilde{\mathcal{Y}} = \bar{\Lambda} - \frac{\partial}{\partial x_i}(\widetilde{\bar{\rho} u_i \mathcal{Y}} - \bar{\rho}\tilde{u}_i\tilde{\mathcal{Y}}). \tag{18}$$

Here our primary interest is in the role of flame stretch which influences the source term. We will not go into the modeling of the unresolved turbulent fluxes.

Let us introduce the surface area convolution of Φ at some position f in the flamelet structure, defined by

$$\langle \Phi_f \rangle = \int_{\partial V_f} \Phi dA_f \Bigg/ \int_{\partial V_f} dA_f. \tag{19}$$

In this study, as we will see later, we will use the notation $\langle \Phi_{\mathrm{in}} \rangle$ for the inner layer surface of the flame that is considered. This surface is defined by the inner layer value of the progress variable, $\mathcal{Y} = \mathcal{Y}_{\mathrm{in}}$, which on its turn is defined by the location of $\mathcal{Y}$ at which the maximum heat release occurs. Similarly, we have the subgrid flame surface for f positioned at the inner layer,

$$\bar{\Sigma} = \bar{\Sigma}_{\mathrm{in}} = \bar{\Sigma}_f = \frac{1}{\Delta V}\int_{\partial V_f} dA_f. \tag{20}$$

By analysis of infinitely thin flames and introducing the flame stretch as initially presented in Ref. 3, the filtered values for the infinitely thin and finite thickness parts of the

total consumption rate $\bar{\Lambda}$ can be obtained. The derivation and its assumptions are given in Appendix A. Note that the filter size must be much larger than the flame thickness. The BML part reads

$$\overline{\Lambda^{\mathrm{BML}}} = \langle m_{\mathrm{in}} \rangle \bar{\Sigma}, \tag{21}$$

with $\bar{\Sigma}$ the flame surface density, which corresponds to the size of the inner layer surface per unit volume. The source associated with stretch was obtained by using Eq. (7),

$$\overline{\Lambda^{*}} = m_{\mathrm{in}}^{0} \langle \mathcal{K}a \rangle \bar{\Sigma}, \tag{22}$$

with m_{in} being the local (stretched) mass burning rate and m_{in}^{0} the unstretched value, being a constant for $\mathrm{Le}_i = 1$. From the obtained value of $\bar{\Sigma}$ in an *a priori* study from DNS results (like Ref. 28) now also $\langle \mathcal{K}a \rangle$ and $\langle m_{\mathrm{in}} \rangle$ can be evaluated. If the surface weighted Karlovitz number is much smaller than 1, the flamelet is virtually very thin and we are in the BML regime.

Furthermore, for the addition of both contributions of the overall consumption, by using Eq. (7) in Eq. (21) and combination with Eq. (22), we arrive at

$$\bar{\Lambda} = \langle m_{\mathrm{in}}^{0} \rangle \bar{\Sigma} = m_{\mathrm{in}}^{0} \bar{\Sigma}, \tag{23}$$

which is a remarkable result. The mean burning rate for unstretched flamelet combustion, m_{in}^{0}, is a constant in the case of $\mathrm{Le}_i = 1$, as studied here. Frequently, a correction factor I_0 is used in this expression (see, e.g., Ref. 29 and references therein). Here we show that this factor is equal to unity for $\mathrm{Le} = 1$ and has strong (but limited) stretch conditions. When preferential diffusion effects ($\mathrm{Le}_i \neq 1$) are included this would no longer be the case. This was studied by Hawkes and Chen,[30] who found factors very close to unity for methane combustion, consistent with the present theory, but an 18% faster turbulent consumption for hydrogen combustion. For very strong stretch, a factor deviating from unity may be required but it should generally not be a constant. In actual LESs also a model is required to determine the flame surface density; this gives some uncertainty. There is a small effect of tangential diffusion of species other than the progress variable. Its impact is an order of magnitude smaller compared to the present stretch effects (see Ref. 31).

Under the given conditions m_{in}^{0} is constant and associated with both the chemical production and the unstretched displacement speed. Then the result implies that the influence of flame stretch on the overall consumption rate is only felt by means of the size of the flame surface density $\bar{\Sigma}$, at which the mean burning rate is constant and equal to the laminar unstretched value m_{in}^{0}.

As can be seen in Appendix A, Eq. (23) is an approximation which is becoming exact for very thin reaction layers or for closed surfaces. Then the gross effect of local leakage of fuel, tangentially along the flame front by means of stretch, is averaged out to be zero. So locally stretch has its influence on the mass burning rate but the integral of the leakage over the actual flame surface is zero. This is the physical interpretation of Eq. (23).

For actual subgrid modeling of the unclosed terms in the equation for the progress variable, the flame surface density is required and the unresolved fluxes have to be modeled. The reader is referred to Ref. 32 for flame surface density models.

Now we will investigate the behavior of the different contributions to $\bar{\Lambda}$ by introducing a filter which is larger than the flame structure. Here the filter size is equal to the domain size. Since we consider flame kernels, the flame front is closed and Eq. (23) is exact in the limit of very thin reaction layers. Note that for the limit of the flame thickness being much smaller than the integration length it is exact as well and this condition is also satisfied. All mentioned quantities can be monitored as a function of time. In particular, we can see how the flame mean Karlovitz integral behaves as a function of time and its relation to a statistically defined Karlovitz number. In principle the flame mean Karlovitz integral $\langle \mathcal{K}a \rangle$ is unknown but it can be evaluated by combination of Eqs. (22) and (23), if these are known,

$$\langle \mathcal{K}a \rangle = \frac{\overline{\Lambda^{*}}}{\bar{\Lambda}} = \frac{\overline{\Lambda^{*}}}{\overline{\Lambda^{*}} + \overline{\Lambda^{\mathrm{BML}}}}. \tag{24}$$

When $\langle \mathcal{K}a \rangle$ approaches 1, the BML contribution becomes negligible compared to stretch effects. All fuel leaks away tangentially to the flame surface and the mass burning rate as given by Eq. (7) goes to zero. In that case flamelet structures will cease to exist and the inner layer is disrupted severely. Eventually, if Karlovitz integrals exceed unity, negative BML values would be possible. The strong stretch model as presented is not suitable for this regime; however, we believe that quite high values of $\langle \mathcal{K}a \rangle$ are accessible, as long as the inner layer stays intact. The physical interpretation of the theory is reflected again in Eq. (24). For negative stretch, at the other side of the spectrum, i.e., flame sheet contraction, $\langle \mathcal{K}a \rangle$ may assume negative values, resulting in an increased mass burning rate.

III. SIMULATIONS AND RESULTS

A. Setup of cases

Fully compressible DNSs are carried out using FGM, based on a single progress variable, for a turbulent spherical premixed flame on a 254^3 grid in a 1.2^3 cm^3 box. Details of the code are described in Ref. 33. The mass fraction of carbon dioxide, which is monotonously increasing, is used as single controlling variable $\mathcal{Y} = Y_{\mathrm{CO_2}} / Y_{\mathrm{CO_2}}^{\mathrm{burnt}}$. The entire set of equations that are solved is given in Ref. 34. Also, initial and boundary conditions are treated in more detail. The fuel consists of methane, premixed with air at an equivalence ratio of 0.7. Preferential diffusion of the chemical species is minimal in this case and not taken into account, $\mathrm{Le}_i = 1$, consistent with the theory. In principle this is not a restriction of the method, but it will simplify the analysis considerably, since turbulent stretch and curvature effects will not be obscured by it, as described in Sec. II. An initially laminar flame kernel was obtained from a time dependent, 1D spherical calculation with detailed chemistry (using the CHEM1D code)[35] up to an inner layer radius of $r = 2.9$ mm. Similar simulations of

TABLE I. Physical properties corresponding to the different simulations.

Case	u'/S_d	l_T/δ_f	Re	Da	Ka
C1	4.0	1.66	6.6	0.42	6.1
C2	8.0	1.66	13.3	0.20	18.2
C3	8.0	3.31	26.6	0.42	12.3

turbulent flame kernels have been carried out in a number of papers[14–16] and measurements have been reported in Ref. 17.

Starting conditions are assumed to be atmospheric, i.e., a pressure of 1 atm and temperature of 300 K. With the specification of these conditions and specifying a kinetic scheme for the chemistry, the burning velocity of a flat unstretched flame with respect to the unburnt mixture, S_d^0, is a fixed physical quantity. In the present study, the chemical kinetics is based on the GRI3.0 scheme. Then the numerical value of the laminar burning velocity is given by $S_d^0=18.75$ cm/s, the corresponding mass burning rate is $m_{\text{in}}^0=0.213$ kg/m^2 s, and the (temperature gradient) flame thickness is $\delta_f=0.614$ mm. With this flame thickness at unstretched conditions the flame is resolved with 13 points.

The initial laminar flame kernel was subjected to a turbulent flow environment. The turbulence was generated by prescribing random numbers to a stream function. This stream function was spatially filtered, converted to a velocity field, and rescaled to obtain the proper velocity scales for an incompressible flow. The length scale is determined by the spatial filtering of the stream function. Note that the 3D streamfunction is only used for initialization purposes. The actual integration is performed on the primitive variables, consisting of density, velocity, and temperature (see Refs. 33 and 34).

The relative turbulence intensities are $u'/S_d=4$ and $u'/S_d=8$ and the length scale ratio was varied from $l_T/\delta_f=1.66$ to $l_T/\delta_f=3.31$. Here the relevant turbulent length scale is defined as the longitudinal integral scale L. In Table I the three considered cases C1– C3 are given. The Karlovitz number Ka is an indicator for flamelet behavior to be valid or not (see Ref. 9). The global Karlovitz number is defined as $\text{Ka}=\sqrt{\text{Re}}/\text{Da}$, with the turbulent Reynolds number $\text{Re}=u'l_T/S_d\delta_f$ and the Damköhler number $\text{Da}=S_d l_T/u'\delta_f$. Usually the turbulent length scale is an integral scale. The Taylor scale is a measure for energy containing eddies. Since in the present case there is not much spectral resolution between this scale and the domain size, the Taylor scale is taken as a measure for the integral length scale. It would mean that probably the Reynolds number is underestimated and the Damköhler and Karlovitz numbers are overestimated.

As a first prerequisite for the simulations and for the subsequent analysis, the flame should be well resolved, which is the case with the chosen parameters. Moreover, the effects of flame stretch and curvature on the local and turbulent burning velocity should be well recovered with the present FGM. In a previous study,[13] on 1D flame propagation with detailed chemistry and FGM it was found that FGM does not decrease grid requirements but it reduces stiffness and chemical complexity in DNS.

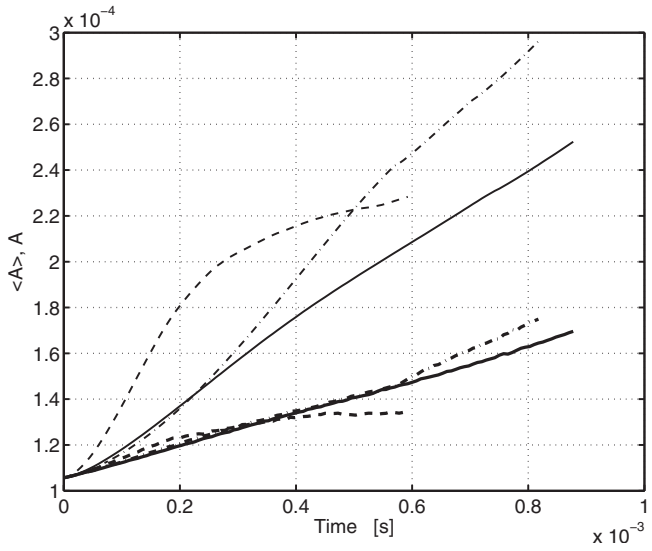

FIG. 1. Surface area of the inner layer value of the progress variable as a function of time. Averaged surfaces (lower three thick lines) and turbulent surfaces (upper three thin lines) for case C1 (drawn), C2 (dashed), and C3 (dot-dashed).

B. Resulting flame structures

From the cases considered, first the flame surface evolution was analyzed. A distinction is made between the averaged flame surface and the turbulent flame surface. The latter is just the actual surface area defined by the inner layer progress variable and it is evaluated by the method described in Ref. 36. For the present lean methane air flame without preferential diffusion the inner layer is positioned at $Y_{\text{cv}}^{\text{il}}=Y_{\text{CO}_2}^{\text{il}}=0.605$. The averaged flame surface is defined as the mean flame radius corresponding to all observations of the progress variable that have a value within a range of $0.98Y_{\text{cv}}^{\text{il}}<Y_{\text{cv}}<1.02Y_{\text{cv}}^{\text{il}}$.

Results of the surface evaluation as a function of time are given in Fig. 1. The end of the lines is defined by the moment at which at some point the flame structure reaches the boundaries of the simulation domain. From the figure it can be observed clearly that the increase in turbulent flame surface area depends on l_T/u'. Cases C1 and C3 have the same value of the turbulent time scale, l_T/u', and at least the initial part of the surface increase is similar. In case C2 the turbulent time scale is halved and, consequently, in the beginning the surface increases two times as fast.

To obtain some more insight into the actual structures we will have a look at the obtained turbulent flame realizations at two instants in time, T_1:$t=0.3$ ms and T_2:$t=0.5$ ms. These times correspond to the time at which, for T_1, cases C1 and C3 still have a common result in terms of flame surface, quite different from C2, and for T_2 which marks the point just after the beginning of the transient in C3 and it coincides with the end of simulation C2.

In Fig. 2 contour plots are given for the progress variable

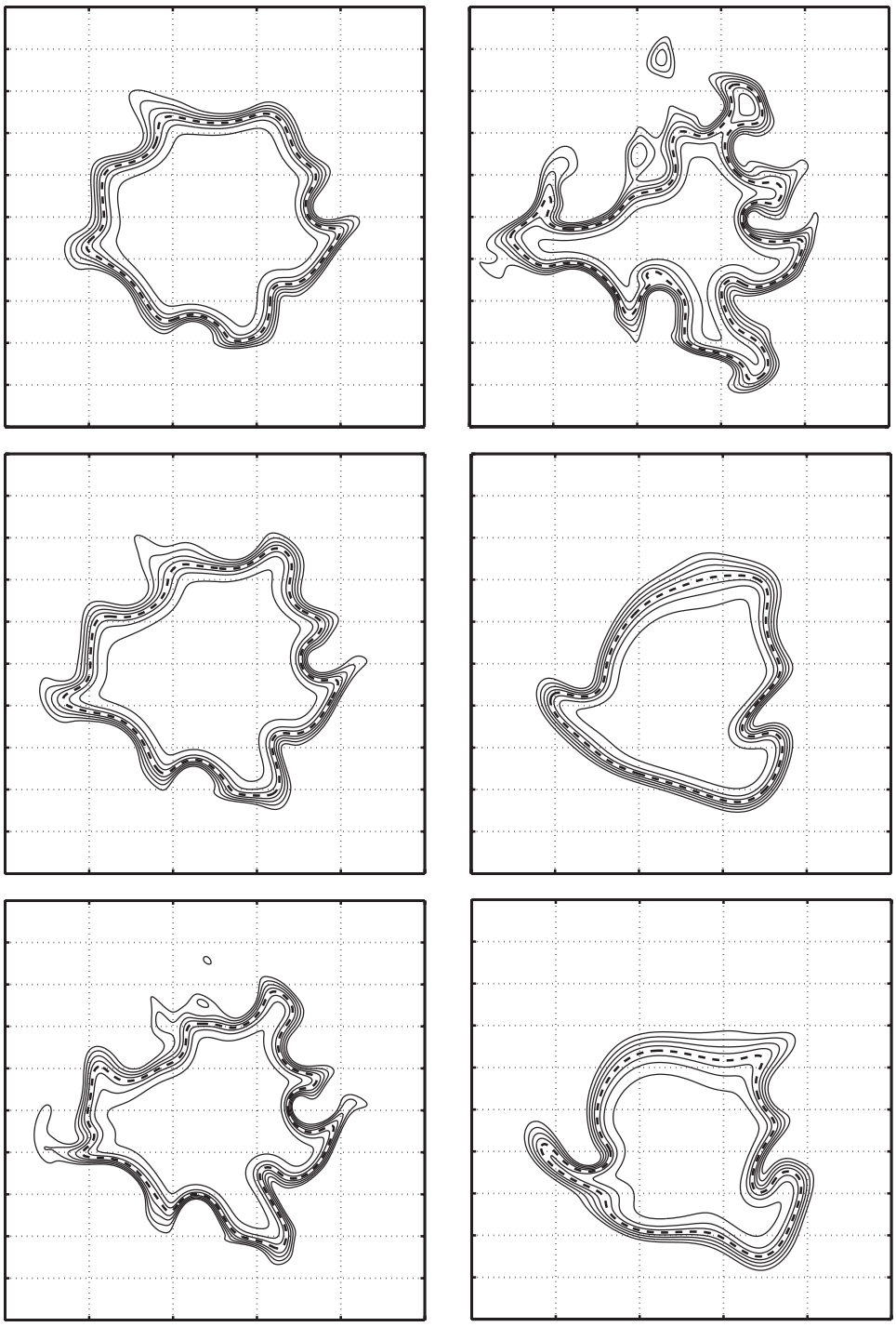

FIG. 2. Contour plots of the progress variable in a central cross section, top to bottom: cases C1, C2, and C3, respectively; left: time T_1, right: time T_2. The values of the contours are given by (drawn) 0.2, 0.3, 0.4, 0.5, 0.7, 0.8, and 0.9 and (dashed) 0.605 (inner layer).

at the given two incidents in time. The figure shows a more or less expected behavior. From the beginning the flame structure starts to deform from an initially perfect sphere. This progresses in time as can be observed from the plots. Additionally, it can be seen that in case C2 the layer at the unburnt side of the inner layer, also known as the preheat zone, is disrupted. Here the preheat zone deviates from a neatly layered structure. This is caused by the more vigorous turbulence in combination with having turbulent kinetic energy in relatively small length scales; this is not observed anymore in case C3. Here, with case C2, we have clearly entered the "thin reaction zone" regime in which the preheat zone is perturbed but the reaction layer is still more or less intact. Note that the initial generation of turbulent fluctuations was the same for all three cases; case C2 shows more amplified deviations and case C3 shows low pass equivalents of the phenomena in cases C1 and C2.

C. Strong stretch analysis

This section deals with the evaluation of quantities as described in Sec. II. Recall that the model will be validated by integral analysis over the entire flame structure. Therefore, this could be interpreted as an *a priori* study over a

single volume, defined by the domain size. Thus the ratio of filter size and flame thickness is about 20. The advantage of this strategy is that the edges of the flame surface at volume boundaries and the associated leakage do not play a role because the flame surface is closed within the volume. Furthermore, enough turbulent realizations are included in the volume to represent turbulent phenomena, governing the flame surface and its preheat zone with sufficient statistics. Therefore, it is believed that the present analysis is adequate to validate the model.

In the assessment first the flame surface density Σ as defined by the inner layer surface of the progress variable is determined. For this and further analysis we change the progress variable to the scaled mass fraction to methane, $\mathcal{Y}=1-Y_{\mathrm{CH}_4}/Y_{\mathrm{CH}_4}^{\max}$. This progress variable is more appropriate for the analysis because it defines a thin reaction layer, for which the inner layer value is positioned at $\mathcal{Y}=0.946$, which is in line with the assumptions made in the theory (it does not change the inner layer position). This in contrast with the progress variable of the FGM method in the DNS (in which we took the scaled CO_2 profile) for which we prefer to have a very smooth profile for $\mathcal{Y}$ that is easily resolved. In determining Σ, at the same time the mass burning rate $\langle m_{\mathrm{in}}\rangle$ is integrated over the surface by means of the method described in Ref. 36. Before doing this the mass burning rate has to be determined in the entire domain according to Eq. (12).

At this moment the total consumption rate and the BML part, $\overline{\Lambda^{\mathrm{BML}}}$, are known. The part of the consumption rate associated with flame stretch, $\overline{\Lambda^*}$, cannot be evaluated directly because the mean Karlovitz integral at the inner layer, $\langle \mathcal{K}a\rangle$, is not *a priori* known. A way to determine $\overline{\Lambda^*}$, which was used here, is to integrate $\rho K\mathcal{Y}$ over the domain [see Eq. (15)]. However, this results in some problems related to the determination of the burning velocity, since it is not well defined in both the unburnt and burnt regions. This is due to the fact that there are no gradients of the progress variable anymore, and the source term is zero as well. A complicating factor is that the derivative of m has to be taken to determine the stretch rate field. Therefore, we limit the integration to the preheat zone up to the inner layer value of the progress variable, which is very close to unity. It was found that the exact boundary does not play a noticeable role.

With the previously described methods both the contributions to the total consumption rate as well as the total consumption rate have been determined independently of each other. Therefore, a first validation would be to check whether the contributions add up to the total. A second validation can be carried out by integrating the left-hand side of Eq. (17) over the domain to determine the total consumption. Here again we have the advantage of the closed flame kernel, which results in the fact that the integral convection term becomes zero, so that $\overline{\Lambda}=(\partial/\partial t)\overline{\rho\mathcal{Y}}$.

The results of all previously determined quantities are displayed in Fig. 3 for the three cases considered. Initially the different contributions are the same for each case and it just defines the consumption of a perfectly spherical flame at the initial radius. After the initiation a transient occurs in which turbulence starts to interact with the flame surface.

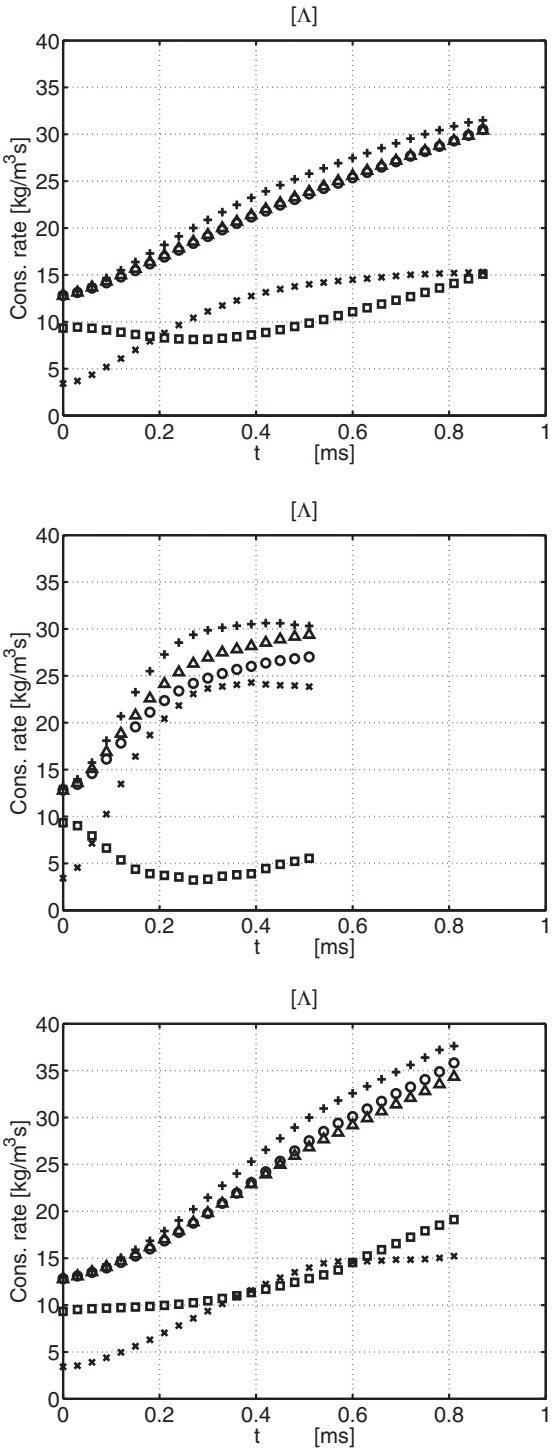

FIG. 3. Mean sources of consumption rate as a function of time: top case C1, middle C2, and bottom C3. Circles denote the total consumption rate $\overline{\Lambda}$ evaluated directly with Eq. (23), squares are the BML contributions, $\overline{\Lambda^{\mathrm{BML}}}$, determined with Eq. (21), the crosses are the contributions of stretch, $\overline{\Lambda^*}$, determined by integrating Eq. (15) over the domain, the plusses are values of $(\partial/\partial t)(\rho\mathcal{Y})$, integrated over the domain, and the triangles are given by $\overline{\Lambda^{\mathrm{BML}}}+\overline{\Lambda^*}$ as given by the squares and crosses.

According to the different physical conditions a clear difference can be observed in the evolution of the total consumption rate. The conclusions about the time scales as drawn from discussing Fig. 1 can be drawn here again. Here the main differences are related to the contributions of flame

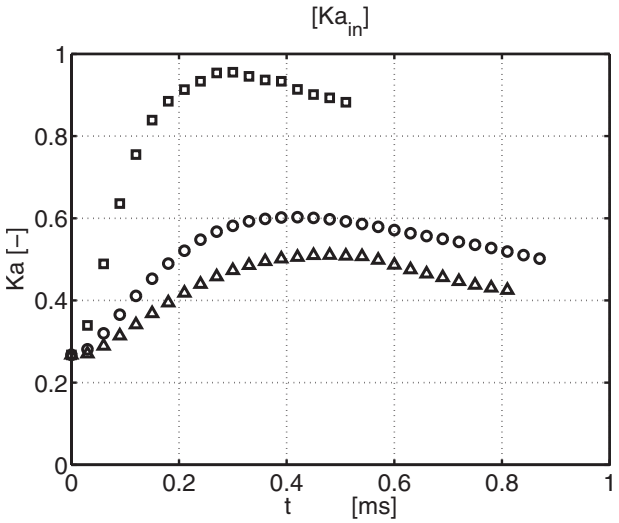

FIG. 4. Mean Karlovitz integral $\langle \mathcal{K}a \rangle$ as a function of time for the different cases: C1 circles, C2 squares, and C3 triangles.

stretch that can be observed. In cases C1 and C3 flame stretch effects remain relatively low, but in case C2 there is a very large contribution of stretch accompanied by a diminished $\overline{\Lambda}^{\mathrm{BML}}$ part. This is associated with the higher Ka number of this case.

The validity of the model can be assessed by looking at the independently determined values of the total consumption. It can be observed that cases C1 and C3 show a very good agreement. Especially in terms of the closure of the budget, the values are in excellent agreement. There is some deviation with the time derivative of the mean mass density, but it is not very large. For case C2 the differences are somewhat larger but they are still quite acceptable in view of modeling such a complicated structure. Evidently the theory breaks down at high Karlovitz numbers at which turbulence starts to penetrate the inner layer of the flame. It has to be mentioned that the resolving capabilities of the surface integration might explain the larger differences at larger Ka. This issue is further explored in Appendix B. From that analysis it is concluded that the analysis is sufficiently accurate. Thus for case C2 the flamelet assumption starts to lose its validity. However, the model is still a fair approximation.

In order to look somewhat closer in the part at which the theory breaks down the mean Karlovitz integrals at the inner layer have been evaluated as a function of time by means of relation (24). The results are depicted in Fig. 4. Here it can be observed that the mean Karlovitz integrals approach unity for case C2. Therefore, local realizations will exceed the $\langle \mathcal{K}a \rangle = 1$ limit considerably and the flamelet regime will not be valid any longer. In view of this result the correlations of the stretch model with actual values can still be considered as being very good.

A third additional validation is provided by flamelet analysis of the flame kernel as in Ref. 6 where we construct flame paths in a direction normal to the progress variable. At these flamelets all the fields necessary to evaluate Eq. (8) are interpolated; subsequently, the local Karlovitz integral at the inner layer, $\mathcal{K}a$, is evaluated. Statistics are determined for each case at the two times, $T_1 = 0.3$ ms and $T_2 = 0.5$ ms. In Table II mean and standard deviations are given. An assessment of the mean values, $\langle \mathcal{K}a \rangle$, reveals that the numbers are in good agreement with Fig. 4. For case C1 the mean values at the two times, T_1 and T_2, are the same in both predictions. The flamelet analysis shows 8%–10% higher values. For case C2 a decrease is given by both methods when going from T_1 to T_2. Again with the flamelets a higher value is found, 17% and 4% higher for T_1 and T_2, respectively. Also for case C3 a slightly increasing trend is predicted by both methods, in case of the flamelet analysis about 17% higher. A slightly biased sampling of the flame surface in combination with the high rms values might explain the relatively small differences. Moreover, an impression of the fluctuations is given, which are relatively high for all cases. The trends for the three cases are clearly distinct and reproduced by both methods. These trends indicate high values of $\langle \mathcal{K}a \rangle$ for C1 and C3, corresponding to a position inside the thin reaction zone regime. Very high values are obtained for C2 reflecting a position relatively high in the thin reaction zone regime.

TABLE II. Statistics of $\mathcal{K}a$ obtained by flamelet analysis using ≈4000 intersections of the flame kernel.

	T_1		T_2	
Case	Mean	rms	Mean	rms
C1	0.64	0.58	0.65	0.61
C2	1.11	1.05	0.92	0.88
C3	0.56	0.54	0.58	0.50

In addition to the above results for the closed spherical flame, the analyses were also performed for the six half domains that can be defined by cutting the domain in two for each direction. This is an assessment in order to evaluate the effects of having filter kernel boundaries that cut the flame. The results, however, did not change significantly (see Fig. 5). It is not within the scope of this paper to extensively evaluate the effects when going to smaller filter kernels. *A posteriori* tests would require closures for the nonlinear term as well as for subgrid contributions in the momentum and a model for the subgrid scale surface density. Future studies will report on these investigations.

IV. CONCLUSIONS

A theory for the description of strong flame stretch has been introduced in Ref. 3. In the present paper this theory is extended in terms of a subgrid closure for the terms connected to flame propagation in the equation for a progress variable. The total production/consumption term $\overline{\Lambda}$ can be decomposed into a contribution related to the propagation of infinitely thin flames supplemented by a contribution connected to flame stretch, inside the flame structure. It can be concluded that for $\mathrm{Le}_i = 1$ the total consumption is effected by stretch only through a change in flame surface density. This is because it is just the product of the unstretched mass burning rate and the flame surface density, in Eq. (23). Of

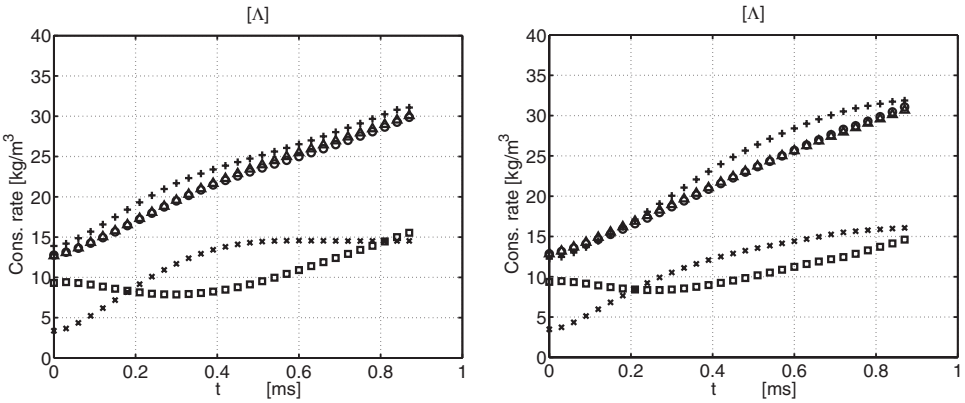

FIG. 5. Influence of intersection of the flame with the filter kernel; mean sources of consumption rate as a function of time for case C1; left: for the lower half of the domain; right: for the upper half. Symbols are as in Fig. 3.

course, locally stretch effects influence the burning velocity of which the total effect is described by a surface mean Karlovitz integral, $\langle \mathcal{K}a \rangle$. Physically the change in local mass burning rate is governed by fuel leakage in the direction tangentially to the flame surface.

The model is validated by means of DNSs in which all the propagation contributions to the subgrid consumption are evaluated. Two independent evaluations of the model values are used for validation. Besides a slight mismatch between the two the agreement is excellent, showing the validity of the theory. An additional validation method based on flamelet tracking also confirms the results of the theory.

ACKNOWLEDGMENTS

The authors thank Bernard Geurts for the surface analysis code, the Dutch Technology Foundation (STW) under Grant No. EWO.5874, and the support of NCF, the Netherlands Computing Facilities Foundation.

APPENDIX A: DERIVATION OF THE VOLUME FILTERED SOURCE TERM

In this appendix we will look at the transport of $\rho\mathcal{Y}$, which is filtered with a top hat filter kernel. This in order to arrive at the appropriate source terms for its grid filtered transport equation.

Let us look at a flamelet-type structure which is contained in a grid volume; see Fig. 6. The grid volume ΔV consists of three parts, V_u, V_b, and V_{ub}. The volume V_{ub} is the volume inside the thin flamelet structure where $\mathcal{Y}$ increases from 0 to 1. We will make use of a short notation $V_f = V_{ub} + V_b$ for the region where the progress value has a nonzero value and thus $\Delta V = V_u + V_f$. It should be mentioned that each isoplane $\mathcal{Y}$ in V_{ub} has its own kinematic velocity u_i^f which is generally not equal to the value for the $\mathcal{Y}=1$ surface, ∂V_b.

With the application of a top hat filter we can write

$$\frac{\partial}{\partial t}\bar{\rho}\tilde{\mathcal{Y}} = \frac{\partial}{\partial t}\overline{\rho\mathcal{Y}} = \frac{\partial}{\partial t}\left(\frac{1}{\Delta V}\int_{\Delta V}\rho\mathcal{Y}dV\right) = \frac{1}{\Delta V}\frac{d}{dt}\int_{V_f}\rho\mathcal{Y}dV, \tag{A1}$$

where $\partial/\partial t = d/dt$ because the boundary ∂V of the control volume ΔV is fixed in space as a function of time. Moreover, because of this, the d/dt can be taken into the integral, which, by application of Reynolds transport theorem, results in

$$\frac{\partial}{\partial t}\bar{\rho}\tilde{\mathcal{Y}} = \frac{1}{\Delta V}\int_{V_f}\frac{d}{dt}(\rho\mathcal{Y})dV \tag{A2}$$

$$= \frac{1}{\Delta V}\int_{V_f}\left(\frac{\partial}{\partial t}\rho\mathcal{Y} + \frac{\partial}{\partial x_j}\rho\mathcal{Y}u_j^f\right)dV. \tag{A3}$$

Furthermore, we have the local flame speed u_j^f, which is equal to $u_j^f = u_j + S_d n_j$, S_d being a field quantity. In principle the burning velocity only has a meaning in regions where the gradient of $\rho\mathcal{Y}$ is not equal to zero. If this gradient is zero we assume that both the flame speed and the burning velocity are zero and the decomposition is not valid anymore. Introduction of this decomposition and with the kinematic equation and continuity,

$$\frac{\partial\mathcal{Y}}{\partial t} + u_j^f\frac{\partial\mathcal{Y}}{\partial x_j} = 0, \quad \frac{\partial\rho}{\partial t} + \frac{\partial\rho u_j}{\partial x_j} = 0, \tag{A4}$$

the right-hand side of Eq. (A3) can be written as

$$\frac{1}{\Delta V}\int_{V_f}\left(-\rho S_d n_j\frac{\partial\mathcal{Y}}{\partial x_j} - \frac{\partial}{\partial x_j}(\rho u_j\mathcal{Y}) + \frac{\partial\rho\mathcal{Y}u_j^f}{\partial x_j}\right)dV. \tag{A5}$$

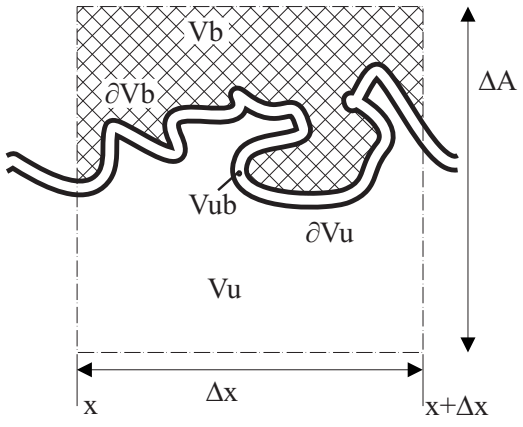

FIG. 6. The averaging volume $\Delta V = \Delta A \Delta x$ for a flamelet with finite thickness; V_u, V_b, and V_{ub} refer to the partial volumes in which $\mathcal{Y}$ is 0, 1, and otherwise, respectively. ∂V_u and ∂V_b are the flamelet boundaries at the unburnt and burnt flamelet sides.

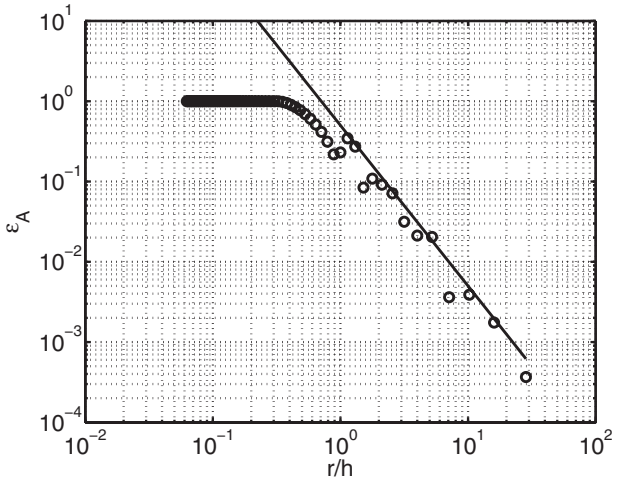

FIG. 7. Accuracy of the surface integration as a function of the resolution, determined by generation of perfect spheres. The drawn line indicates a second order convergence, $\epsilon_A=0.5(r/h)^{-2}$.

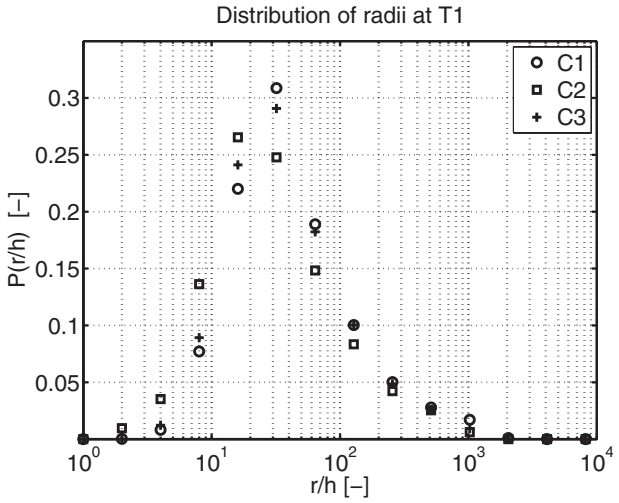

FIG. 8. Distribution of radii at the inner layer on the basis of flamelet analysis, using the local curvature. Results are for different cases: at time T_1 (there is not much change going to time T_2). The local radius is estimated (conservatively) on the basis of spherical curvature, $r=2/\kappa$. Absolute values of the radii are displayed.

Now we can rewrite the left-hand side of the transport equation to be equal to

$$\frac{\partial}{\partial t}\bar{\rho}\tilde{\mathcal{Y}}+\frac{\partial}{\partial x_j}\overline{\rho u_j\mathcal{Y}}=\frac{1}{\Delta V}\int_{V_f}\left(-\rho S_d n_j\frac{\partial\mathcal{Y}}{\partial x_j}+\frac{\partial\rho\mathcal{Y}u_j^f}{\partial x_j}\right)dV. \tag{A6}$$

The first term in the right-hand side only contributes in the region V_{ub}; in the other regions $\mathcal{Y}$ is constant, either 0 or 1. The second term can be written as a surface flux. This flux only has a value at the intersections of the external surface with the flame region V_{ub} (at the other parts of the surface the gradients of $\rho\mathcal{Y}$ are equal to zero).

So for flame surfaces that are internally closed in the filter volume, there are no intersections of the flame with the kernel boundaries. In that case the second term in the right hand side of Eq. (A6) is equal to zero. If, on the other hand, the flame intersects with the boundary, as is the general case which is depicted in Fig. 6, the part of the kernel boundary adjacent to V_{ub} has a normal contribution when the local flame has a boundary tangential component. Statistically, the probability of the value of this term is symmetric around zero; fluxes going in or going out are as likely. If we assume that the flame structures are very thin, these contributions will vanish. Therefore, the entire second term can be dropped resulting in

$$\frac{\partial}{\partial t}\bar{\rho}\tilde{\mathcal{Y}}+\frac{\partial}{\partial x_j}\widetilde{\bar{\rho}u_j\mathcal{Y}}=-\frac{1}{\Delta V}\int_{V_{ub}}mn_j\frac{\partial\mathcal{Y}}{\partial x_j}dV=\bar{\Lambda}, \tag{A7}$$

in which ρS_d, the local mass burning rate, is written as m, and the convection, at the left-hand side, is again written in Favre averaged quantities.

This result could have been obtained as well by taking the convolution of Eq. (11) as in Eq. (17), using a top hat filter kernel over $\Delta V=\Delta A\Delta x$. The detailed derivation, however, gives a clear insight into the assumptions that have to be made.

Now the chain rule for the right-hand side of Eq. (A7) defines the decomposition as given in Eq. (13). Then the first integral is

$$\overline{\Lambda^{\mathrm{BML}}}=-\frac{1}{\Delta V}\int_{V_{ub}}\frac{\partial}{\partial x_j}(mn_j\mathcal{Y})dV=\frac{1}{\Delta V}\int_{\partial V_b}mdA_b, \tag{A8}$$

which, with the definitions Eqs. (19) and (20) can be written as

$$\overline{\Lambda^{\mathrm{BML}}}=\langle m_b\rangle\bar{\Sigma}_b. \tag{A9}$$

This result explains why we refer to this contribution as the Bray, Moss, and Libby term. It can be seen that only one single flame surface, ∂V_b, is responsible for this term. This is in agreement with their theory since ultimately all internal flame structure is canceled out. Inherently it cannot describe detailed flame stretch effects. This also results in an expression containing the averaged stretched mass burning rate $\langle m_b\rangle$, which is unknown.

The second integral is then the pure contribution of stretch inside V_{ub}, which with Eq. (6) becomes

$$\overline{\Lambda^*}=\frac{1}{\Delta V}\int_{V_{ub}}\mathcal{Y}\frac{\partial}{\partial x_j}mn_jdV=\frac{1}{\Delta V}\int_{V_{ub}}\rho K\mathcal{Y}dV, \tag{A10}$$

and with the Karlovitz integral, Eq. (8) and Eqs. (19) and (20) we obtain

$$\overline{\Lambda^*}=\frac{1}{\Delta V}\int_{A_f}m^0\mathcal{K}adA_f=\langle m^0\mathcal{K}a\rangle\bar{\Sigma}_f. \tag{A11}$$

Since we have taken an integral over the flame thickness the position of f is not exactly defined anymore but it should be contained in V_{ub}. This also holds for the position b in Eq. (A9), in which the flame thickness is not an issue. The best defined position then is the inner layer, the position where the heat release is maximal.

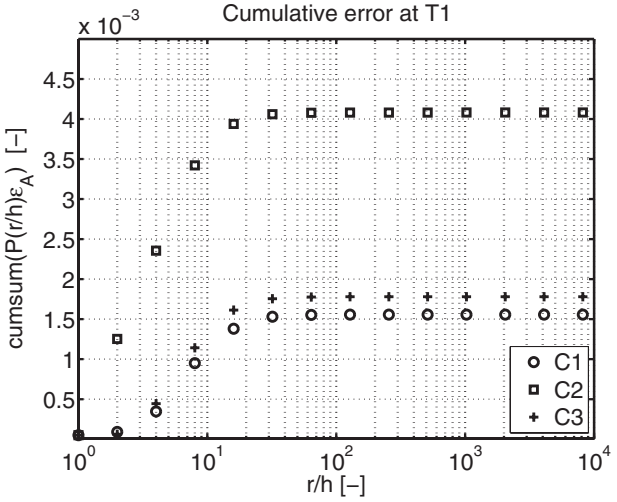

FIG. 9. Cumulative error, defined as the cumulative sum of the product of the error line (solid line in Fig. 7 times the probability distribution of Fig. 8).

We end with assembling everything to

$$\frac{\partial}{\partial t}\bar{\rho}\tilde{\mathcal{Y}} + \frac{\partial}{\partial x_j}\bar{\rho}\widetilde{u_j\mathcal{Y}} = \bar{\Lambda} = \overline{\Lambda^{\mathrm{BML}}} + \overline{\Lambda^*}$$

$$= \langle m_{\mathrm{in}} + m_{\mathrm{in}}^0 \mathcal{K}a\rangle \bar{\Sigma}_{\mathrm{in}} = \langle m_{\mathrm{in}}^0\rangle \bar{\Sigma}_{\mathrm{in}} = m_{\mathrm{in}}^0 \bar{\Sigma}. \tag{A12}$$

APPENDIX B: ACCURACY OF THE ANALYSES OF THE DNS DATA

In this appendix an assessment of the accuracy of the surface integrals is given. In all cases we made sure that the resolution of the basic DNS calculations was sufficient. However, the postprocessing analysis for determining surface integrals had a lower formal accuracy. In cases C1 and C3 the theory is valid if the accuracy of the analysis is sufficient. In case C2 either the theory starts to lose its validity or the analysis is not accurate enough or both.

The accuracy of the surface integrals is assessed by investigating the prediction of the amount of surface for perfect spheres. Errors are determined as a function of the resolution, in which r is the radius of the sphere and h is the numerical grid size. In Fig. 7 the errors are displayed. At $r/h=2$ errors have already dropped to 10%. For reference a $0.5(r/h)^{-2}$ line is drawn to show the second order accuracy of the postprocessing method. This line is used as a conservative estimation of the accuracy in the next step of the analysis.

From the figure we can see that the accuracy of the surface integrals is limited for large curvatures (small radii), which especially occur in case C2. It is expected that the surface integration in which the integrand is a field variable, being nonunity as in the present case (in case of determination of $\langle m_{\mathrm{in}}\rangle$), the resolution is even more limited.

To interpret the previously obtained result in the context of the present evaluations, the distribution of radii, occurring in the fields that are obtained in the DNSs, is determined. Now this can be estimated by using the flamelet tracking method. With this method flame paths normal to local $\mathcal{Y}$ isocontours are determined through the flame front. All variables relevant for the analysis are interpolated on the flame paths. This results in flamelets, in which combustion variables are determined as a function of their respective paths through the flame front. One of the variables that can be subject to this tracking technique is the local curvature of the progress variable field, as defined by the derivative of the flame normals,

$$\kappa = \frac{\partial n_i}{\partial x_i}, \tag{B1}$$

the flame normals being the derivatives of the progress variable, $n_i = \partial\mathcal{Y}/\partial x_i$. From this we can assess the radii occurring. For doing this a numerical method for determining the derivatives is required that is both accurate and compact. Here we use a sixth order compact Padé scheme, which is consistent with the methods used in the simulations.

The flamelets can be determined at a large number of locations. In principle, if this number is large enough, the set of obtained flamelets can be considered to be representative for the entire flame surface. However, flamelet starting points are at discrete grid points that are close to the inner layer, at the unburnt side where curvature is relatively large, but not necessarily at the inner layer. This means that regions of high curvature will be slightly under-represented. Since we take many flamelets (typically 50 000) we assume that this effect is only of minor importance.

Results of the curvature distribution using this flamelet analysis are presented in Fig. 8. Clearly, as expected, case C2 has the smallest structures. At the smallest structures the differences between the cases are also the largest. We can combine the occurrence of curvatures in Fig. 8 with the accuracy for a certain curvature from Fig. 7. A cumulative plot of this is displayed in Fig. 9. Here we can see that the accuracy of the method is quite good. Furthermore, the accuracy is determined by scales smaller than $30h$. Although the errors of case C2 are higher than the analysis errors in cases C1 and C3, they are still very small. This leads us to the conclusion that the model starts to lose its validity at case C2, but as can be seen in the main text, it is still a fair approximation.

[1] M. Matalon and B. J. Matkowsky, "Flames as gas dynamic discontinuities," J. Fluid Mech. **124**, 239 (1982).
[2] P. Clavin and F. A. Williams, "Effects of molecular diffusion and of thermal expansion on the structure and dynamics of premixed flames in turbulent flows of large scale and low intensity," J. Fluid Mech. **116**, 251 (1982).
[3] L. P. H. de Goey and J. H. M. ten Thije Boonkkamp, "A flamelet description of premixed laminar flames and the relation with flame stretch," Combust. Flame **119**, 253 (1999).
[4] J. A. van Oijen, "Flamelet-Generated Manifolds: Development and Application to Premixed Laminar Flames," Ph.D. thesis, Eindhoven University of Technology, 2002.
[5] O. Gicquel, N. Darabiha, and D. Thevenin, "Laminar premixed hydrogen/air counter flow flame simulations using flame propagation of ILDM with preferential diffusion," Proc. Combust. Inst. **28**, 1901 (2000).
[6] J. A. van Oijen, R. J. M. Bastiaans, G. R. A. Groot, and L. P. H. de Goey, "A flamelet analysis of the burning velocity of premixed turbulent expanding flames," Proc. Combust. Inst. **30**, 657 (2005).

[7]J. A. van Oijen, G. R. A. Groot, R. J. M. Bastiaans, and L. P. H. de Goey, "Direct numerical simulations of premixed turbulent flames with reduced chemistry: validation and flamelet analysis," Flow, Turbul. Combust. **75**, 67 (2005).
[8]J. A. van Oijen, R. J. M. Bastiaans, and L. P. H. de Goey, "Low-dimensional manifolds in direct numerical simulations of premixed turbulent flames," Proc. Combust. Inst. **31**, 1377 (2007).
[9]N. Peters, *Turbulent Combustion* (Cambridge Monographs on Mechanics, Cambridge University Press, 2000).
[10]J. F. Driscoll, "Turbulent premixed combustion: Flamelet structure and its effect on turbulent burning velocities," Prog. Energy Combust. Sci. **34**, 91 (2008).
[11]F. Halter, C. Chauveau, I. Gökalp, "Investigations on the flamelet inner structure of turbulent premixed flames," Combust. Sci. Technol. **180**, 713 (2008).
[12]L. P. H. de Goey, T. Plessing, R. T. E. Hermanns, and N. Peters, "Analysis of the flame thickness of turbulent flamelets in the thin reaction zones regime," Proc. Combust. Inst. **30**, 859 (2005).
[13]R. J. M. Bastiaans, J. A. van Oijen, and L. P. H. de Goey, "Application of flamelet-generated manifolds and flamelet analysis of turbulent combustion," Int. J. Multiscale Comp. Eng. **4**, 307 (2006).
[14]*Direct Numerical Simulation for Turbulent Reacting Flows*, edited by T. Baritaud, T. Poinsot, and M. Baum (Edition Technip, Paris, 1996).
[15]K. W. Jenkins and R. S. Cant, "Curvature effects on flame kernels in a turbulent environment," Proc. Combust. Inst. **29**, 2023 (2002).
[16]D. Thévenin, "D., Three-dimensional direct numerical simulations and structure of expanding turbulent methane flames," Proc. Combust. Inst. **30**, 629 (2005).
[17]S. Gashi, J. Hult, K. W. Jenkins, N. Chakraborty, R. S. Cant, and C. F. Kaminski, "Curvature and wrinkling of premixed flame kernels-comparisons of OH PLIF and DNS data," Proc. Combust. Inst. **30**, 809 (2005).
[18]N. Chakraborty, M. Klein, and R. S. Cant, "Stretch rate effects on displacement speed in turbulent premixed flame kernels in the thin reaction zones regime," Proc. Combust. Inst. **31**, 1385 (2007).
[19]K. W. Jenkins, M. Klein, N. Chakraborthy, and R. S. Cant, "Effects of strain rate and curvature on the propagation of a spherical flame kernel in the thin-reaction-zones regime," Combust. Flame **145**, 415 (2006).
[20]M. Klein, N. Chakraborthy, K. W. Jenkins, and R. S. Cant, "Effects of initial radius on the propagation of premixed flame kernels in a turbulent environment," Phys. Fluids **18**, 055102 (2006).
[21]T. Echekki and H. Kolera-Gokula, "A regime diagram for premixed flame kernel-vortex interactions," Phys. Fluids **19**, 043604 (2007).
[22]H. Kolera-Gokula and T. Echekki, "Direct numerical simulation of premixed flame kernel-vortex interactions in hydrogen-air mixtures," Combust. Flame **146**, 155 (2006).
[23]D. C. Haworth and T. J. Poinsot, "Numerical simulations of Lewis number effects in turbulent premixed flames," J. Fluid Mech. **244**, 405 (1992).
[24]R. W. Bilger, S. B. Pope, K. N. C. Bray, and J. F. Driscoll, "Paradigms in turbulent combustion research," Proc. Combust. Inst. **30**, 21 (2005).
[25]G. R. A. Groot and L. P. H. de Goey, "A computational study of propagating spherical and cylindrical premixed flames," Proc. Combust. Inst. **29**, 1445 (2002).
[26]J. A. M. de Swart, G. R. A. Groot, J. A. van Oijen, J. H. M. ten Thije Boonkkamp, and L. P. H. de Goey, "Detailed analysis of the mass burning rate of stretched flames including preferential diffusion effects," Combust. Flame **145**, 245 (2006).
[27]K. N. C. Bray, P. A. Libby, and B. J. Moss, "Flamelet crossing frequencies and mean reaction rates in premixed turbulent combustion," Combust. Sci. Technol. **41**, 143 (1984).
[28]M. Boger, D. Veynante, H. Boughanem, and A. Trouvé, "Direct numerical simulation analysis of flame surface density concept for large eddy simulation of turbulent premixed combustion," Proc. Combust. Inst. **27**, 917 (1998).
[29]K. N. C. Bray, "Studies on the turbulent burning velocity," Proc. R. Soc. London, Ser. A **431**, 315 (1990).
[30]E. R. Hawkes and J. H. Chen, "Comparison of direct numerical simulation of lean premixed methane-air flames with strained laminar flame calculations," Combust. Flame **144**, 112 (2006).
[31]J. H. M. ten Thije Boonkkamp, L. P. H. de Goey, J. A. van Oijen, A. Class, and Y. Bronner, "Two quasi-one dimensional descriptions on premixed flames based on flame coordinates," Combust. Sci. Technol. **180**, 1449 (2008).
[32]T. Poinsot and D. Veynante, *Theoretical and Numerical Combustion* (Edwards, Ann Arbor, 2001).
[33]R. J. M. Bastiaans, L. M. T. Somers, and H. C. de Lange, *Modern Simulation Strategies for Turbulent Flow*, edited by B. J. Geurts (Edwards, Philadelphia, 2001), pp. 247–261.
[34]R. J. M. Bastiaans, J. A. van Oijen, S. M. Martin, L. P. H. de Goey, and H. Pitsch, "DNS of lean premixed turbulent spherical flames with a flamelet generated manifold," CTR Annual Research Briefs, Center for Turbulence Research, Stanford, 2004, pp. 257–268.
[35]L. M. T. Somers, "Simulation of flat flames with detailed and reduced chemical models," Ph.D. thesis, Eindhoven University of Technology, 1994.
[36]B.J. Geurts, "Mixing efficiency in turbulent shear layers," J. Turbul. **2**, 1 (2001).